

Manifestations of interference fluctuations of phase functions and backscattering cross sections for ice crystals with specific orientations

G Guo¹, P Yang^{1,5}, Y X Hu², D Winker², C A Hostetler², B A Baum²
and J Reichardt^{3,4}

¹ Department of Atmospheric Sciences, TAMU 3150, Texas A & M University, College Station, TX 77843, USA

² NASA Langley Research Center, MS 420, Hampton, VA 23681, USA

³ Joint Center for Earth Systems Technology, University of Maryland Baltimore County, Baltimore, MD 21250, USA

⁴ Code 916, NASA Goddard Space Flight Center, Greenbelt, MD 20771, USA

E-mail: pyang@ariel.met.tamu.edu

Received 26 February 2003, accepted for publication 4 July 2003

Published 28 July 2003

Online at stacks.iop.org/JOptA/5/520

Abstract

The ray-by-ray integration technique is applied to investigate the effect of the phase interference between rays on the scattering phase functions and backscattering cross sections of pristine hexagonal ice plates and columns with specific orientations. Numerical computations are carried out at 0.532 and 1.064 μm wavelengths. The results demonstrate that strong fluctuations of the phase function as a function of scattering angle are inherent for oriented particles. In addition, constructive fluctuation patterns are noted for particle backscattering cross sections, and are a function of particle size. These fluctuations, which are absent from the conventional ray-tracing computations, are caused by phase interference.

Keywords: Phase interference, scattering, ice crystals

1. Introduction

Knowledge of the scattering characteristics of ice crystals is critical to the study of cirrus clouds [1, 2]. Two quantities, the scattering phase function and backscattering cross section, are important parameters for retrieving the properties of cirrus clouds from satellite-based measurements from instruments such as the Moderate Resolution Imaging Spectrometer (MODIS) [3], the dual-viewing Along Track Scanning Radiometer (ATSR-2) [4], the Polarization and Directionality of Earth Reflectance (POLDER) [5], and the future Cloud–Aerosol Lidar and Infrared Pathfinder Satellite Observations (CALIPSO, formerly named PICASSO-CENA) [6]. Baran *et al* [7] have shown the fundamental importance of the

scattering phase function and backscattering cross sections of ice crystals in the retrieval of cirrus microphysical and bulk properties using ASTR-2 data. Note that the ATSR-2 is a dual-viewing instrument and thus allows sampling of the cirrus cloud at two different scattering angles. Numerous observations (e.g., [8]) show that ice crystals are almost exclusively nonspherical particles. Pristine ice crystals, the predominant crystal habits at extremely cold cloud temperatures, are normally hexagonal plates or columns. The 22° and 46° haloes observed in the atmosphere are attributed to the hexagonal structure of these particles. The scattering properties of ice crystals with small and moderate size parameters (defined as $\pi D_e/\lambda$, where D_e is the effective diameter defined in [9], following the original work of Foot [10], and λ is the incident wavelength) have been investigated using the *T*-matrix method [11, 12] and the finite-

⁵ Author to whom any correspondence should be addressed.

difference time domain (FDTD) method [13]. For large size parameters, the scattering properties of ice crystals have been investigated by using the ray-tracing method and other approximate methods [14–19]. Recently, a generalization of the separation-of-variables method (SVM) has been developed and applied to finite noncircular cylinders by Rother [20, 21]. This method has been used to study the scattering properties of the hexagonal ice column [22, 23].

Ice crystals in the atmosphere are normally larger than $20 \mu\text{m}$ in terms of their maximum dimensions. For the scattering of visible and near-infrared radiation by these ice crystals, the corresponding size parameters are in the applicable regime of geometric optics, i.e., when the size parameter is greater than 40 [24, 25]. Hence the conventional ray-tracing technique [14] can be employed to calculate the single-scattering properties of large ice crystals. Phase interference between rays is often neglected in the conventional ray-tracing method. Although the effect of ray interference is minimized when ice crystals are randomly oriented, it can be pronounced for ice crystals with specific orientations. Recent improvements in the scattering computational methods based on the principles of geometric optics allows a full accounting for the phase interference. For example, Stamnes and his colleagues (e.g., [26, 27]) developed the combined method of ray tracing and diffraction (CMRD) that accounts effectively for the phase information. The CMRD has been applied to the diffraction analysis of optical systems and also to the modelling of light scattering.

Because cirrus tends to exist in the upper troposphere where strong horizontal winds are present, moderate and large pristine ice crystals tend to have preferred orientations in the atmosphere due to aerodynamic considerations. Orientation of ice crystals in the upper troposphere can also be due to the imposition of electric fields [28]. The oriented ice crystals in the atmosphere have been observed by a satellite instrument called POLDER [5] as well as ground-based lidar [29]. The goal of the present study is to better understand the effect of the phase interference on the scattering properties of pristine ice crystals with specific orientations. The ray-by-ray integration (RBRI) technique [30] is applied to compute the scattering phase functions and backscattering cross sections of oriented hexagonal plates and columns.

2. Single-scattering properties of ice plates and columns with specific orientations

For the ensuing analysis, three coordinate systems are defined: the particle coordinate system, the incident ray coordinate system, and the scattering system. The particle system, $OX_p Y_p Z_p$, is fixed to the scattering particle of interest. This coordinate system rotates with the particle. The incident ray coordinate system $OX_i Y_i Z_i$ specifies the direction and polarization configuration of the incident radiation. The OZ_i -axis points along the incident direction whereas OX_i and OY_i denote the two orthogonal directions for specifying the polarization configuration of the incident wave. The scattering coordinate system, $OX_s Y_s Z_s$, specifies scattered light. The OZ_s -axis is selected along the propagating direction of scattered light.

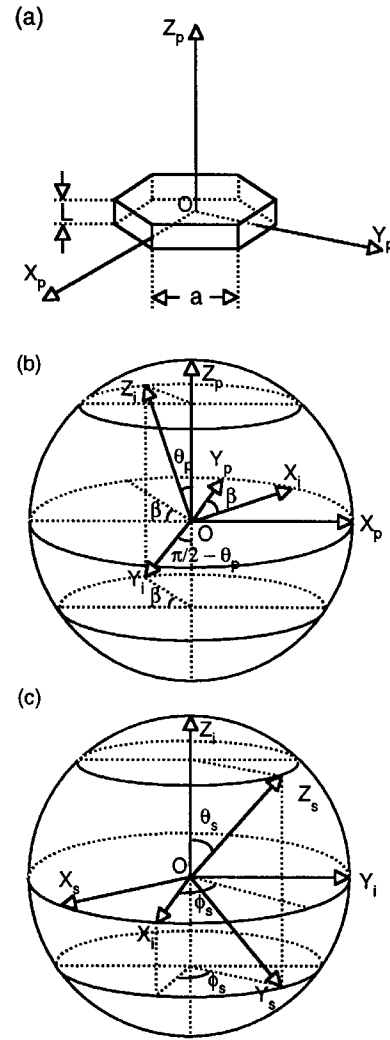


Figure 1. Geometries of pristine hexagonal ice plates and columns. Also shown are the coordinate systems defined for incidence and scattering configurations.

Figure 1 shows the configurations of the three coordinate systems. It can be shown that the coordinate transformation from the incident ray coordinate system to the particle coordinate system may be given by

$$\begin{pmatrix} X_p \\ Y_p \\ Z_p \end{pmatrix} = \begin{pmatrix} \sin \beta & -\cos \theta_p \cos \beta & -\sin \theta_p \cos \beta \\ \cos \beta & \cos \theta_p \sin \beta & \sin \theta_p \sin \beta \\ 0 & -\sin \theta_p & \cos \theta_p \end{pmatrix} \begin{pmatrix} X_i \\ Y_i \\ Z_i \end{pmatrix}, \quad (1)$$

where two angles, θ_p and β , are indicated in figure 1(b). In equation (1), X_p , Y_p , and Z_p are specified with respect to the particle system whereas X_i , Y_i , and Z_i are specified with respect to the incident coordinate system.

The coordinate transformation from the scattering coordinate system to the incident coordinate system is given by

$$\begin{pmatrix} X_i \\ Y_i \\ Z_i \end{pmatrix} = \begin{pmatrix} \sin \phi_s & \cos \theta_s \cos \phi_s & \sin \theta_s \cos \phi_s \\ -\cos \phi_s & \cos \theta_s \sin \phi_s & \sin \theta_s \sin \phi_s \\ 0 & -\sin \theta_s & \cos \theta_s \end{pmatrix} \begin{pmatrix} X_s \\ Y_s \\ Z_s \end{pmatrix}, \quad (2)$$

where θ_s is scattering angle, and ϕ_s indicates the azimuthal angle of a scattering plane of interest. θ_s and ϕ_s are indicated

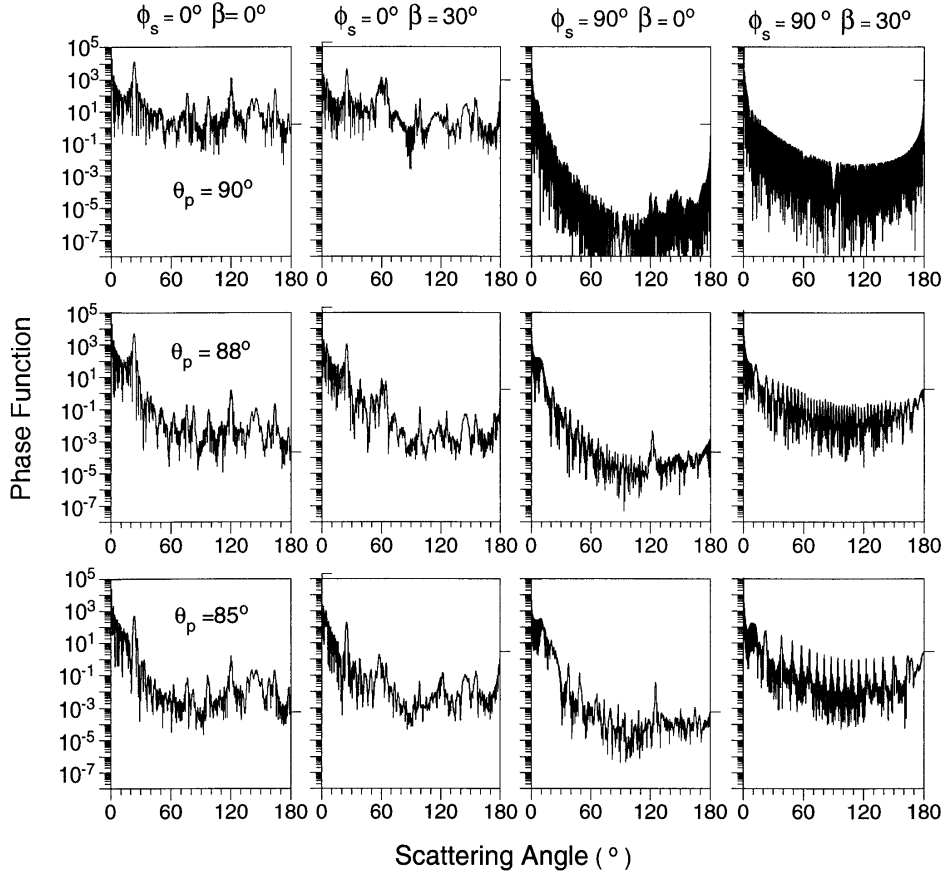


Figure 2. The phase function of an individual hexagonal ice column with an aspect ratio of $D/L = 30 \mu\text{m}/100 \mu\text{m}$ at wavelength $0.532 \mu\text{m}$.

in figure 1(c). In equation (2), X_s , Y_s , and Z_s are specified with respect to the scattering coordinate system.

For light scattering computations, one may equivalently specify the orientation of a particle with respect to the incident coordinate system or specify the incident geometry relative to the particle system. In the present study, we use the latter approach. The coordinate system transformation from the scattering coordinate to the particle coordinate system is given by

$$\begin{pmatrix} X_p \\ Y_p \\ Z_p \end{pmatrix} = \begin{pmatrix} \sin \beta & -\cos \theta_p \cos \beta & -\sin \theta_p \cos \beta \\ \cos \beta & \cos \theta_p \sin \beta & \sin \theta_p \sin \beta \\ 0 & -\sin \theta_p & \cos \theta_p \end{pmatrix} \times \begin{pmatrix} \sin \phi_s & \cos \theta_s \cos \phi_s & \sin \theta_s \cos \phi_s \\ -\cos \phi_s & \cos \theta_s \sin \phi_s & \sin \theta_s \sin \phi_s \\ 0 & -\sin \theta_s & \cos \theta_s \end{pmatrix} \begin{pmatrix} X_s \\ Y_s \\ Z_s \end{pmatrix}. \quad (3)$$

The RBRI technique [30] is based on the combination of an electrodynamic integral equation and the principles of geometric optics. It was developed in an attempt to extend the applicable regime of the conventional ray-tracing method to moderate size parameters. In the ray-by-ray integration method, the internal field inside the scattering particle is calculated by using the principles of geometric optics. The far field corresponding to the internal field is computed by mapping the near field via the following relationship that relates the near field within the particle to the far field:

$$\begin{aligned} \vec{E}^s(\vec{r})|_{kr \rightarrow \infty} &= \frac{k^2 e^{ikr}}{4\pi r} (\varepsilon - 1) \\ &\times \int \int \int_v \{ \vec{E}(\vec{r}') - \hat{r}[\hat{r} \cdot \vec{E}(\vec{r}')] \} e^{-ik\hat{r} \cdot \vec{r}'} d^3 r'. \end{aligned} \quad (4)$$

With the coordinate transformation matrices defined in equations (1)–(3) and the electromagnetic integral relationship in equation (4), the scattering matrix $S(\hat{r})$ can be written as follows:

$$S(\hat{r}) = \sum_r \sum_{n=1}^N S_n(\hat{r}), \quad (5a)$$

$$S_n(\hat{r}) = \frac{ik^3(1 - \varepsilon)}{4\pi} q_n(\hat{r}) K_n U_n \Gamma, \quad (5b)$$

where $S_n(\hat{r})$ denotes the contribution of an internal ray within the particle to the scattering matrix. The subscript n in the above equations denotes the order of the internal ray, and N is the maximum order of the internal rays considered in the ray-tracing calculation, which is taken as $N = 8$ in the present computation. The summation over index r in equation (5a) denotes the summation of the contribution of all the incident rays. Note that the ray refracted into the particle is denoted as the first-order internal ray, the ray having undergone one internal reflection is denoted as the second-order internal ray, and so on. The detailed description regarding the derivation of equation (5) from (4) can be found in Yang and Liou [24].

In equation (5a), which is in a form that is suitable for numerical computations, U_n is a 2-by-2 matrix involving a set

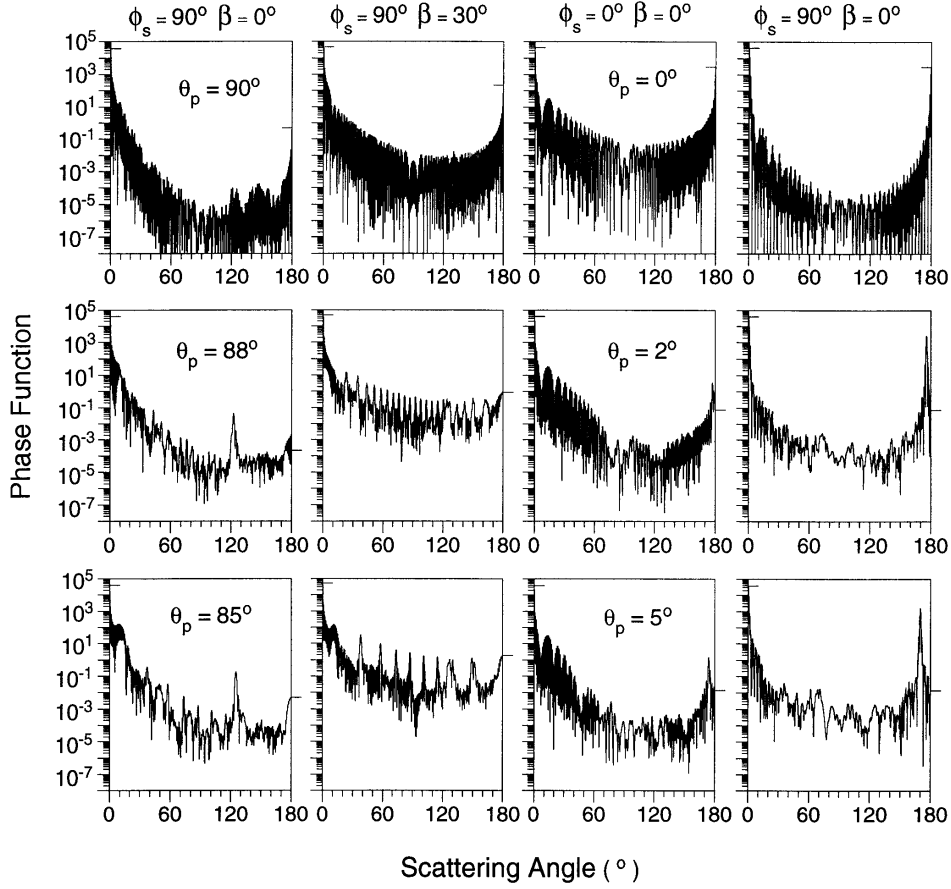


Figure 3. The phase function of a hexagonal ice column with an aspect ratio of $D/L = 20 \mu\text{m}/40 \mu\text{m}$ and plate with an aspect ratio of $D/L = 50 \mu\text{m}/10 \mu\text{m}$ at wavelength $\lambda = 0.532 \mu\text{m}$.

of recursive equations that account for the Fresnel reflection (or refraction) coefficients and the rotational transformation of the field expressions with respect to the plane of incidence, Γ is a 2-by-2 rotational matrix that transforms the field expressions from the scattering plane to the incident plane, K_n is a matrix associated with the projection of the electric field of a localized wave onto the components parallel and perpendicular to the scattering plane, and $q_n(\hat{r})$ is calculated by integrating the phase of a ray along its path. The total scattering matrix $S(\hat{r})$ in equation (5b) is obtained by summing the contributions of all the localized waves or geometric optics rays and the contributions of different initial or incident rays. Further technical details regarding the implementation of the ray-by-ray integration technique are provided in Yang and Liou [30]. Some validation of this method has been performed through comparison to both the rigorous FDTD method in Yang and Liou [30] and experimental data in Liou *et al* [1].

After the amplitude scattering matrix is defined, the scattering cross section σ_s , phase function P_{11} , and lidar backscattering cross section σ_b can be obtained as follows:

$$\sigma_s = \frac{1}{2k^2} \int_0^\pi \int_0^{2\pi} (|S_1|^2 + |S_2|^2 + |S_3|^2 + |S_4|^2) \sin \theta_p \, d\theta_p \, d\varphi_p, \quad (6)$$

$$P_{11} = \frac{2\pi}{k^2 \sigma_s} (|S_1|^2 + |S_2|^2 + |S_3|^2 + |S_4|^2), \quad (7)$$

$$\sigma_b = \sigma_s P_{11}(\theta_s = 180^\circ). \quad (8)$$

The S_1 , S_2 , S_3 , and S_4 in equations (6) and (7) are the four elements of the amplitude scattering matrix in equation (5a), given by

$$S = \begin{pmatrix} S_2 & S_3 \\ S_4 & S_1 \end{pmatrix}. \quad (9)$$

3. Numerical results and discussions

For an ice crystal with a given maximum dimension, we define the three-dimensional geometry of the particle by using the aspect ratios reported by Auer and Veal [31] for plates and Yang *et al* [9] for columns, which are

$$L = 2.020a^{0.449} \quad \text{for plates}, \quad (10)$$

and

$$a = \begin{cases} \frac{L}{2}, & L \leq 40 \mu\text{m}, \\ \frac{L}{2} e^{-0.017835(L-40)}, & 40 < L < 50 \mu\text{m}, \\ 2.958L^{1/2}, & L > 50 \mu\text{m}, \end{cases} \quad \text{for columns}, \quad (11)$$

where a is the semi-width of the cross section and L is the length (for a column) or thickness (for a plate) of the ice crystal. The present numerical computations are carried out for phase functions and backscattering cross sections of ice

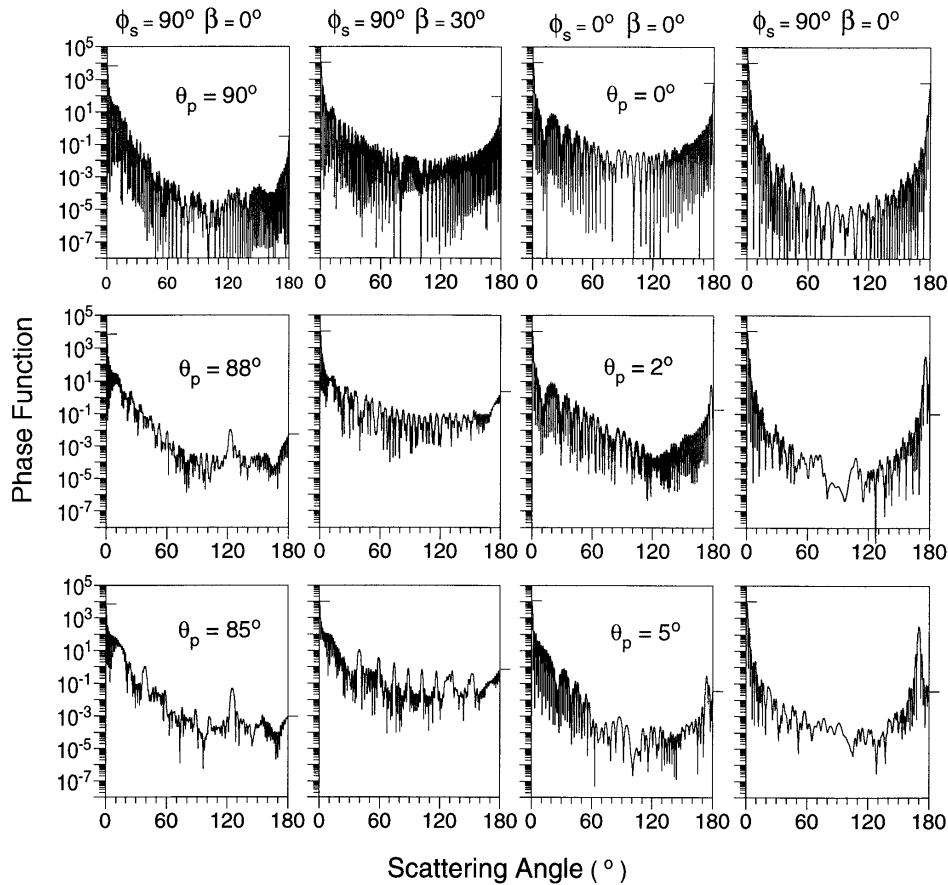


Figure 4. As figure 3, but $\lambda = 1.064 \mu\text{m}$.

plates and columns at 0.532 and $1.064 \mu\text{m}$ wavelengths. In the numerical computations, the incident direction denoted by the OZ_i -axis of the incident coordinate system is assumed to point upward vertically, i.e., in the direction of the zenith. The polarization of the incident wave with respect to the particle is specified by the OX_i - and OY_i -axes of the incident coordinate system. The scattering characteristics of ice crystals at these two wavelengths are important for understanding both the extinction-to-backscatter ratio and multiple-scattering effects in the lidar measurements.

Figure 2 shows the phase functions at $0.532 \mu\text{m}$ wavelength for a column with an aspect ratio of $D/L = 30 \mu\text{m}/100 \mu\text{m}$, in which $D = 2a$ is the width of the cross section of the particle. The refractive indices of ice at these two wavelengths are $1.3117 + i2.6138 \times 10^{-9}$ and $1.3004 + i1.933 \times 10^{-6}$ [32]. The short horizontal bars in the diagrams indicate the magnitudes of the phase functions in the forward-scattering and backscattering directions. Some of the error bars in the forward directions cannot be seen because the magnitudes of those phase functions in the forward direction are close to 10^5 (i.e., those horizontal bars overlap the tick marks). The upper row in figure 2 is for the case where the symmetric axis of the column is oriented horizontally. The second and third rows are for the cases where the symmetric axis of the column is tilted 88° and 85° from the zenith, respectively. The phase functions are quite sensitive to the orientations of ice columns. A very strong scattering peak at 22° is noted for results shown in the left two columns of

figure 2. This peak is associated with the hexagonal structure typical of pristine ice crystals. Additionally, a scattering peak at 120° is noted for certain orientations of ice columns. This peak originates from the two internal reflections of the incident beam inside the hexagonal columns. One pronounced feature displayed in figure 2 is that the phase functions fluctuate substantially as functions of scattering angle. The fluctuations are caused by the phase interference of various rays emerging in the same scattering directions. This unique feature is absent in the results obtained from the conventional ray-tracing techniques.

Figure 3 shows the phase functions at wavelength $0.532 \mu\text{m}$ for columns with an aspect ratio of $D/L = 20 \mu\text{m}/40 \mu\text{m}$ and plates with an aspect ratio of $D/L = 50 \mu\text{m}/10 \mu\text{m}$. Note that the size of the columns used in the calculations for figure 3 is smaller than that of those used in figure 2. The results for the two sizes of columns are similar, as is evident from the comparison of the left two columns in figure 3 with the right two columns in figure 2. The upper row in the right two columns in figure 3 is for the case where the symmetric axis of the plate is vertically oriented and the second and third rows are for the cases where the symmetric axis of the plate is tilted 2° and 5° from the zenith. For plates, strong backscattering may result if the particles are horizontally oriented, that is, $\theta_p = 0^\circ$. When the symmetric axis is tilted from the zenith, strong peaks near the backscattering direction are noted. These peaks correspond to the specular reflection from the basal faces of the plates.

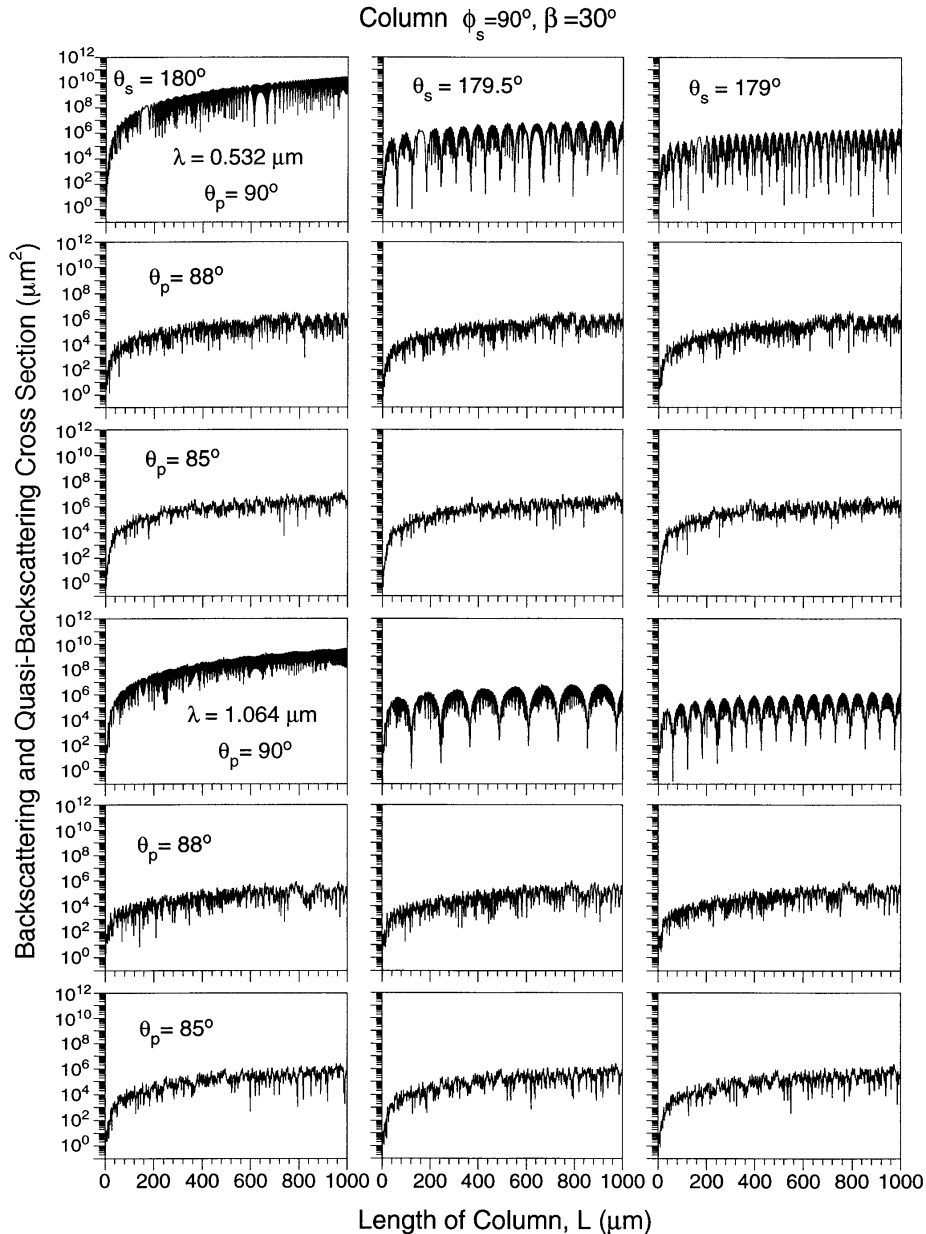


Figure 5. The variation of backscattering and quasi-backscattering cross sections of ice columns.

Figure 4 is the same as figure 3 except that calculations are performed at a near-infrared wavelength $\lambda = 1.064 \mu\text{m}$. From comparison of figures 3 and 4, one may note that the fluctuations of the phase functions versus scattering angle for wavelength $\lambda = 0.532 \mu\text{m}$ are more pronounced than those for wavelength $\lambda = 1.064 \mu\text{m}$.

Figures 5 and 6 show the backscattering and quasi-backscattering cross sections of columns and plates as functions of particle maximum size. The quasi-backscattering cross section is defined in a similar manner to that in equation (8), except that the phase function value involved in the quasi-backscattering cross section is not evaluated at the exact 180° scattering angle. In figures 5 and 6, the quasi-backscattering cross section is evaluated at $\theta_s = 179.5^\circ$ and 179° . When the tilting angle of the plate is zero (i.e., $\theta_p = 0^\circ$), or the tilting angle of the column is 90° (i.e., $\theta_p = 90^\circ$), the

quasi-backscattering cross sections for both plates and columns show some constructive oscillation patterns with respect to the particle sizes. Additionally, the quasi-backscattering cross sections are substantially smaller than backscattering cross sections when the tilting angle of the plate is zero or when the tilting angle of the column is vertical. For columns, the constructive oscillation patterns for the quasi-backscattering cross sections reduce to noise-like fluctuations when the symmetric axis of the columns is tilted from the zenith. Unlike columns, plates produce appreciable constructive oscillation patterns for the quasi-backscattering cross section even if the plates are tilted, as is evident from the results shown in figure 6.

4. Summary

We employ the ray-by-ray integration technique to investigate the scattering properties of pristine ice plates and columns

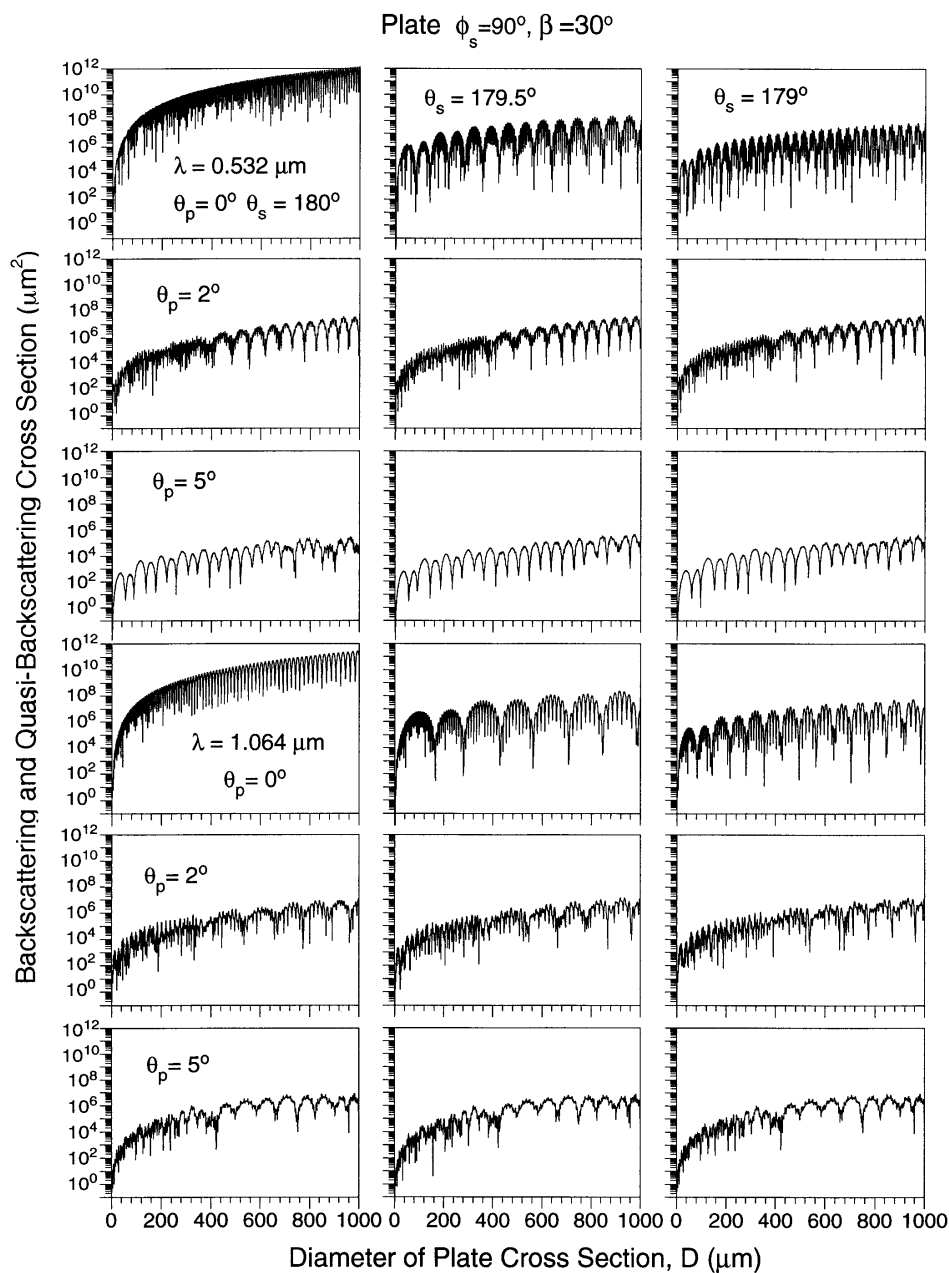


Figure 6. As figure 5, but for ice plates.

with specific orientations at 0.532 and 1.064 μm wavelengths. Numerical computations indicate that common features of all the results are

- (1) the rapid oscillations of the phase functions as a function of the scattering angles and
- (2) the variation of the backscattering or quasi-backscattering cross sections as a function of particle size.

These oscillations are caused by the phase interference of rays. This interesting feature is absent in the results obtained by the conventional ray-tracing technique that ignores the phase variation in the ray-tracing calculations. In general, the oscillations are stronger at wavelength 0.532 μm than at the near-infrared wavelength 1.064 μm , and may be due to the larger size parameters at the visible wavelength. We also note that the backscattering cross sections are sensitive to both wavelength and the

orientation of the ice plates and columns. The present study shows that the effect of phase interference of rays is important for calculating the single-scattering properties of ice crystals with specific orientations.

Acknowledgments

This research was supported by the NASA CALIPSO project, the NASA Radiation Science Program managed by Dr Donald Anderson (NAG5-11374) and the NASA Atmospheric Chemistry Modeling and Analysis Program managed by Dr Phil DeCola.

References

- [1] Liou K N, Takano Y and Yang P 2000 Light scattering and radiative transfer by ice crystal clouds: applications to

- climate research *Light Scattering by Nonspherical Particles: Theory, Measurements, and Geophysical Applications* ed M I Mishchenko, J W Hovenier and L D Travis (New York: Academic) ch 15, p 417
- [2] Hu X Y, Winker D M, Yang P, Baum B A, Poole L and Vann L 2001 *J. Quant. Spectrosc. Radiat. Transfer* **70** 569–79
- [3] King M D, Kaufman Y J, Menzel W P and Tanre D 1992 *IEEE Trans. Geosci. Remote Sens.* **30** 2–27
- [4] Baran A J, Brown S J, Foot J S and Mitchell D L 1998 *J. Geophys. Res.* **103** 6075–82
- [5] Chepfer H, Brogniez G, Goloub P, Breon F M and Flamant P H 1999 *J. Quant. Spectrosc. Radiat. Transfer* **63** 521–43
- [6] Winker D M and Wielicki B A 1999 *Proc. SPIE* **3870** 26–36
- [7] Baran A J, Watts P D and Francis P N 1999 *J. Geophys. Res.* **104** 31673–83
- [8] Heymsfield A J and Iaquinta J 2000 *J. Atmos. Sci.* **57** 916–38
- [9] Yang P, Gao B C, Baum B A, Hu Y X, Wiscombe W J, Tsay S C, Winker D M and Nasiri S L 2001 *J. Quant. Spectrosc. Radiat. Transfer* **70** 473–504
- [10] Foot J S 1988 *Q. J. Meteorol. Soc.* **114** 145–64
- [11] Mishchenko M I, Wielgaard D D and Carlson B E 1997 *Geophys. Res. Lett.* **24** 771–4
- [12] Havemann S and Baran A J 2001 *J. Quant. Spectrosc. Radiat. Transfer* **70** 139–58
- [13] Yang P and Liou K N 1996 *J. Opt. Soc. Am. A* **13** 2072–85
- [14] Takano Y and Liou K N 1989 *J. Atmos. Sci.* **46** 1–19
- [15] Macke A 1993 *Appl. Opt.* **32** 2780–8
- [16] Borovoi A, Grishin I, Naats E and Oppel U 2002 *J. Quant. Spectrosc. Radiat. Transfer* **72** 403–17
- [17] Noel V, Chepfer H, Ledanois G and Flamant P H 2001 *Appl. Opt.* **40** 4365–75
- [18] Yang P and Liou K N 1998 *Contrib. Atmos. Phys.* **71** 223–48
- [19] Reichardt J, Reichardt S, Hess M and McGee T J 2002 Correlations among the optical properties of cirrus-cloud particles: microphysical interpretation *J. Geophys. Res.* **107(D21)** 4562, doi:10.1029/2002JD002589
- [20] Rother T 1998 *J. Quant. Spectrosc. Radiat. Transfer* **60** 335–53
- [21] Rother T, Havemann S and Schmidt K 1999 *Prog. Electromagn. Res.* **23** 79–105
- [22] Rother T 1999 *J. Electromagn. Waves Appl.* **13** 867–88
- [23] Rother T, Schmidt K and Havemann S 2001 *J. Opt. Soc. Am. A* **18** 2512–17
- [24] Yang P and Liou K N 1995 *J. Opt. Soc. Am. A* **12** 162–76
- [25] Mishchenko M I and Macke A 1999 *Appl. Opt.* **38** 1626–9
- [26] Stamnes J J and Heier H 1998 *Appl. Opt.* **37** 3612–22
- [27] Chen B and Stamnes J J 1998 *Appl. Opt.* **37** 1999–2010
- [28] Foster T C and Hallett J 2000 *13th Int. Conf. on Clouds and Precipitation* pp 641–4
- [29] Platt C M, Abshire N L and McNice G T 1977 *J. Appl. Meteorol.* **17** 1220–4
- [30] Yang P and Liou K N 1997 *J. Opt. Soc. Am. A* **14** 2278–89
- [31] Auer A H and Veal D L 1970 *J. Atmos. Sci.* **27** 919–26
- [32] Warren S G 1984 *Appl. Opt.* **23** 1206–25